The SUrvey for Pulsars and Extragalactic Radio Bursts – IV. Discovery and polarimetry of a 12.1-s radio pulsar

V. Morello,[1]* E. F. Keane,[2] T. Enoto,[3] S. Guillot,[4] W. C. G. Ho,[5] A. Jameson,[6,7]
M. Kramer,[1,8] B. W. Stappers,[1] M. Bailes,[6,7] E. D. Barr,[8] S. Bhandari,[9] M. Caleb,[1]
C. M. L. Flynn,[8] F. Jankowski,[1] S. Johnston,[9] W. van Straten,[10] Z. Arzoumanian,[11]
S. Bogdanov,[12] K. C. Gendreau,[11] C. Malacaria,[13,14] P. S. Ray[15] and
R. A. Remillard[16]

[1]*Jodrell Bank Centre for Astrophysics, School of Physics and Astronomy, The University of Manchester, Manchester M13 9PL, UK*
[2]*SKA Organisation, Jodrell Bank Observatory, SK11 9DL, Macclesfield UK*
[3]*Department of Astronomy, Kyoto University, Kitashirakawa-Oiwake-cho, Sakyo-ku, Kyoto 606-8502, Japan*
[4]*CNRS, IRAP, 9 avenue du Colonel Roche, BP 44346, F-31028 Toulouse Cedex 4, France*
[5]*Department of Physics and Astronomy, Haverford College, 370 Lancaster Avenue, Haverford, PA 19041, USA*
[6]*Centre for Astrophysics and Supercomputing, Swinburne University of Technology, PO Box 218, Hawthorn, VIC 3122, Australia*
[7]*OzGrav - ARC Centre of Excellence for Gravitational Wave Discovery, PO Box 218, Hawthorn, VIC 3122, Australia*
[8]*Max-Planck-Institut für Radioastronomie, Auf dem Hügel 69, D-53121 Bonn, Germany*
[9]*CSIRO Astronomy and Space Science, PO Box 76, Epping, NSW 1710, Australia*
[10]*Institute for Radio Astronomy & Space Research, Auckland University of Technology, Private Bag 92006, Auckland 1142, New Zealand*
[11]*X-ray Astrophysics Laboratory, Astrophysics Science Division, NASA's Goddard Space Flight Center, Greenbelt, MD 20771, USA*
[12]*Columbia Astrophysics Laboratory, Columbia University, 550 West 120th Street, New York, NY 10027, USA*
[13]*NASA Marshall Space Flight Center, NSSTC, 320 Sparkman Drive, Huntsville, AL 35805, USA*
[14]*Universities Space Research Association, NSSTC, 320 Sparkman Drive, Huntsville, AL 35805, USA*
[15]*Space Science Division, U.S. Naval Research Laboratory, Washington, DC 20375, USA*
[16]*MIT Kavli Institute for Astrophysics and Space Research, 70 Vassar Street, Cambridge, MA 02139, USA*

ABSTRACT

We report the discovery of PSR J2251−3711, a radio pulsar with a spin period of 12.1 s, the second longest currently known. Its timing parameters imply a characteristic age of 15 Myr, a surface magnetic field of 1.3×10^{13} G, and a spin-down luminosity of 2.9×10^{29} erg s^{-1}. Its dispersion measure of 12.12(1) pc cm^{-3} leads to distance estimates of 0.5 and 1.3 kpc according to the NE2001 and YMW16 Galactic free electron density models, respectively. Some of its single pulses show an uninterrupted 180-deg sweep of the phase-resolved polarization position angle, with an S-shape reminiscent of the rotating vector model prediction. However, the fact that this sweep occurs at different phases from one pulse to another is remarkable and without straightforward explanation. Although PSR J2251−3711 lies in the region of the $P - \dot{P}$ parameter space occupied by the X-ray isolated neutron stars (XINS), there is no evidence for an X-ray counterpart in our *Swift* XRT observation; this places a 99 per cent-confidence upper bound on its unabsorbed bolometric thermal luminosity of 1.1×10^{31} $(d/1 \, \mathrm{kpc})^2$ erg s^{-1} for an assumed temperature of 85 eV, where d is the distance to the pulsar. Further observations are needed to determine whether it is a rotation-powered pulsar with a true age of at least several Myr, or a much younger object such as an XINS or a recently cooled magnetar. Extreme specimens like PSR J2251−3711 help bridge populations in the so-called neutron star zoo in an attempt to understand their origins and evolution.

Key words: stars: neutron – pulsars: general – pulsars: individual: PSR J2251−3711.

1 INTRODUCTION

The standard evolutionary picture of isolated pulsars is that they are born with spin periods of up to a few tens of millisec-

* E-mail: vmorello@gmail.com

onds (Noutsos et al. 2013; Lyne et al. 2015) and, through the loss of rotational energy via electromagnetic radiation and other processes, slow down (see e.g. Lyne & Graham-Smith 2012). The star cools quickly, by an order of magnitude in $\lesssim 10^6$ yr (e.g. Potekhin, Pons & Page 2015), such that older neutron stars are generally difficult or impossible to detect via their thermal X-ray emission. Those that produce radio emission do so for $\sim 10^7$ yr before the emission mechanism quenches (Keane et al. 2013). The exact criteria for cessation of radio emission are not well constrained but are generally considered to be dependent upon the magnetic field strength at the stellar surface and the spin period (Chen & Ruderman 1993). The various models predict a lack of radio emission in the so-called death valley region of the spin period–period derivative $(P - \dot{P})$ parameter space where there is a dearth of sources. Although not accounted for by models, there is mounting observational evidence that the cessation does not happen abruptly, with intermittent emission observed now in several sources (Kramer et al. 2006; Camilo et al. 2012; Young et al. 2014).

Radio pulsars have been found with a wide range of spin periods, stretching from 1.4 ms to 23.5 s (Hessels et al. 2006; Tan et al. 2018), such that there now appears to be a range of spin periods, in the tens of seconds, that is occupied by both radio emitting neutron stars and white dwarfs (Patterson 1979). The millisecond pulsars are understood to have been 'spun up' through interactions with their later-evolving binary partners (Bhattacharya & van den Heuvel 1991). This spin-up process reignites the radio emission process if it has ended; in contrast, isolated pulsars remain dead. It is therefore with the isolated pulsars that one could trace out the true spin evolution post-supernova if their ages could be accurately determined; unfortunately, that is precisely where the difficulty lies. Accurate ages have been obtained via supernova remnant (SNR) associations (Gaensler & Frail 2000; Kramer et al. 2003), or by tracing pulsar trajectories in the Galactic gravitational potential back to their most likely birth site(s), yielding a so-called *kinematic age* (e.g. Noutsos et al. 2013). These methods are not always applicable; SNRs remain detectable only for $\simeq 10^5$ yr, while the derivation of a kinematic age requires at least a proper motion measurement. In the absence of a better alternative, as is commonly the case with older ($\gtrsim 1$ Myr) neutron stars, one has to fall back to the inaccurate but available 'characteristic age' $\tau_c = P/(2\dot{P})$.

Radio pulsars are not the only representatives of isolated neutron stars (INS), which manifest themselves under several sub-types of objects with different observational properties. Two classes are of particular interest here. Magnetars derive their name from the high surface magnetic fields ($B_{surf} \simeq 10^{13} - 10^{15}$ G) implied by their spin-down parameters. They are typically very young ($\simeq 1$–30 kyr) and have spin periods of a few seconds. Their X-ray and soft γ-ray emission is generally accepted to be powered by the dissipation of their intense magnetic fields (Thompson & Duncan 1995; Kaspi & Beloborodov 2017), since their average luminosity often greatly exceeds their rotational energy loss rate. X-ray isolated neutron stars (XINS) are nearby cooling neutron stars characterized by their thermal emission in the soft X-ray band and overall steadiness as sources. Their spin periods lie in the 3–17 s range and their ages are estimated to be of a few hundred kyr (Turolla 2009). XINS have never been seen in the radio domain despite extensive attempts, although this could just be caused by a chance misalignment of their hypothetical radio beams with our line of sight (Kondratiev et al. 2009). The fact that

the radio pulsar PSR J0726−2612 was found to produce thermal emission similar to that of the XINS (Rigoselli et al. 2019) supports the misalignment hypothesis. For a complete overview of the INS diversity, one can refer to a review paper such as Kaspi & Kramer (2016).

Many of the INS class labels are not mutually exclusive and, most importantly, it has been shown that the birth rate of core-collapse supernovae is insufficient to account for all neutron stars being born directly into whichever sub-category they currently belong to; this implies that there must be evolutionary links between at least some classes of INS (Keane & Kramer 2008). Correctly identifying all such possible links is key to achieving what has been previously called the unification of the neutron star zoo (Kaspi 2010). If this is the goal, then it is worth trying to uncover the possible ancestors of the newly emerging population of very slow-spinning radio pulsars.

In this paper we describe, in Section 2, the discovery and subsequent radio observations of PSR J2251−3711, a 12.1-s period radio pulsar. In Section 3, we provide its phase-coherent timing solution and perform detailed analysis of its radio emission characteristics. Section 4 describes the observations of the source in the X-rays with the *Neil Gehrels Swift X-ray Observatory* (Burrows et al. 2005) and the *Neutron Star Interior Composition Explorer (NICER)*. In Section 5, we attempt to constrain the true age of this pulsar and discuss where it may fit in an evolutionary context with respect to the entire population, before drawing our conclusions in Section 6.

2 RADIO OBSERVATIONS

2.1 Discovery

PSR J2251−3711 was discovered in the SUrvey for Pulsars and Extragalactic Radio Bursts (SUPERB, see Keane 2018, for details), conducted with the Parkes 21-cm multibeam receiver (Staveley-Smith et al. 1996). At the time of discovery, SUPERB was using a Fourier-domain search as well as a single pulse search and it was in the latter that the pulsar was first detected, in a 9-min blind survey observation taken on 2015 December 8 (UTC 2015-12-08-10:06:21, beam number 4). Fig. 1 shows the single pulse search diagnostic plots, exhibiting nine pulses detected with signal-to-noise ratios in excess of 10σ and best-fitting widths between 4 and 16 ms. A rudimentary analysis of the differences between pulse times of arrival (TOAs) in this 9-min discovery observation alone initially suggested a best-fitting period of 6.06 s; however, no signal was detected by directly folding the raw data. The true period of 12.12 s was serendipitously found in 2016 January while testing a fast folding algorithm (FFA) search code (then in an early phase of development) in conjunction with a multibeam interference mitigation code. In a 1-h confirmation observation taken on 2016 January 19, the source was seen again with a much higher statistical significance and any remaining doubts on the true period were dissipated.

We also looked for archival observations near the position of PSR J2251−3711, and found that two dispersed pulses from the source were visible in a 4.5-min observation in the high Galactic latitude portion of the High Time Resolution Universe (HTRU; Keith et al. 2010) survey (UTC 2009-05-02-01:08:57, beam number 7). The source likely went undetected in the HTRU single pulse search due to its low dispersion measure (DM = 12.1 pc cm^{-3}, see Section 3.1) making it difficult to distinguish from radio-frequency
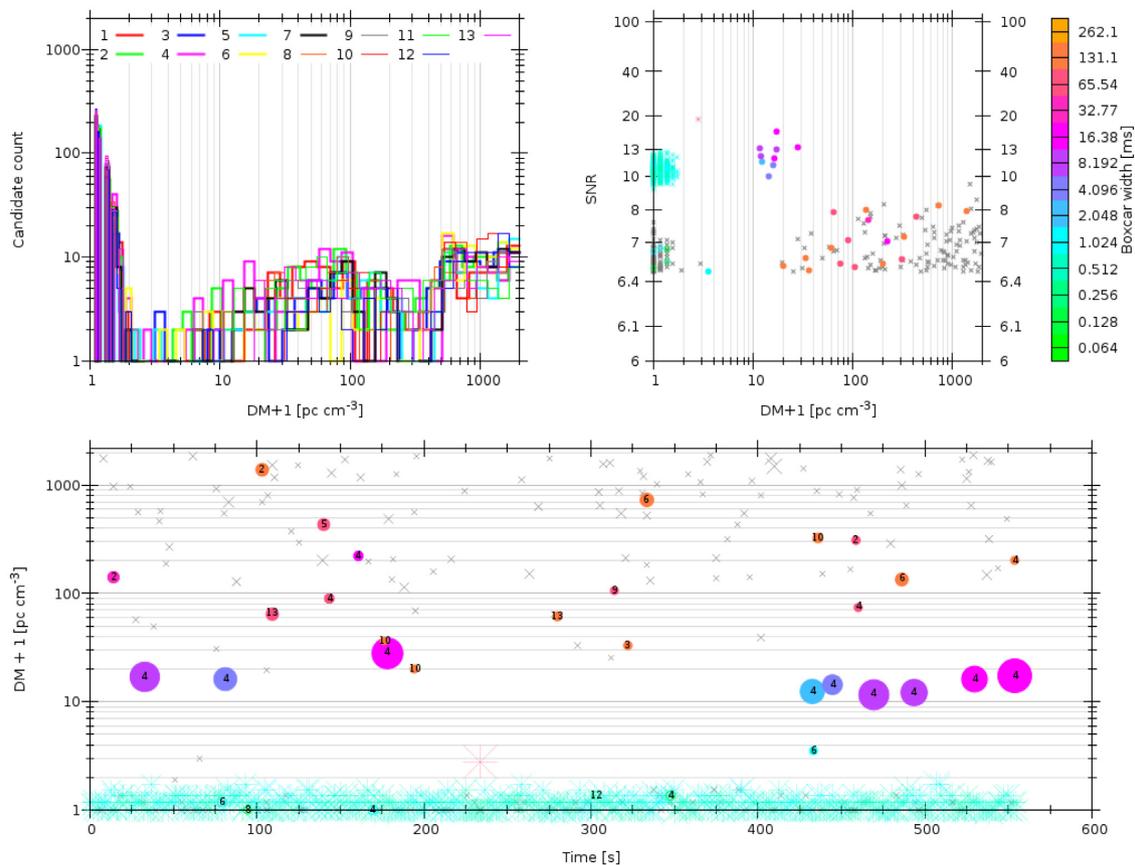
Figure 1. Discovery plot of PSR J2251−3711 as produced by the HEIMDALL single pulse search pipeline. Detected pulses in this 9-min discovery observation are shown as filled circles in the bottom panel in a time–dispersion measure (DM) diagram. The colour denotes the value of the best-fitting pulse width, and the circle size indicates signal-to-noise ratio (SNR). The beam number in which they were detected is overlaid. Top left: DM distributions of detected single pulses, plotted for every individual beam. Top right: detected single pulses in a DM–SNR diagram, for all 13 beams of the receiver.

interference (RFI) that occurs predominantly at DM 0 (Keane et al. 2010).

2.2 Parkes multibeam receiver observations

In order to obtain a phase-coherent timing solution, PSR J2251−3711 has been observed regularly since its discovery whenever the SUPERB project was allocated telescope time at Parkes, except for a 10-month hiatus between 2016 February and December during which the multibeam receiver was taken down for refurbishment. All timing observations were acquired with the Berkeley Parkes Swinburne Recorder (BPSR) backend, using the standard search-mode SUPERB configuration: a 1382 MHz centre frequency, 400 MHz of bandwidth divided in 1024 frequency channels, and a time resolution of 64 μs. Only Stokes I was recorded with 2-bit digitization and integration times were either 18 or 30 min. In addition to the regular timing campaign, a longer 2-h observation was taken on 2018 September 28, where all four Stokes parameters were recorded with the BPSR backend as well, this time with 8-bit precision but with the number of frequency channels reduced to 128 due to system limitations. From this observation, henceforth referred to as *the main observation*, we were able to obtain polarization profiles and perform a number of single pulse analyses.

3 RADIO ANALYSIS

3.1 Dispersion measure and distance estimation

The DM of a pulsar is routinely used to estimate its distance using a model of the Galactic free electron density, the two most recent and widely used being NE2001 (Cordes & Lazio 2002) and YMW16 (Yao, Manchester & Wang 2017). While in most cases the uncertainty on the distance thus derived is dominated by model limitations, in the case of PSR J2251−3711 the dispersion delay between edges of the Parkes multibeam receiver band is approximately half its integrated pulse width. This corresponds to a large fractional error on the DM which therefore contributes significant additional uncertainty to a distance estimate. Indeed, running a period-DM optimization utility such as PSRCHIVE'S pdmp (Hotan, van Straten & Manchester 2004) on the folded main observation yields a best-fitting DM of 15.8 ± 3.6 pc cm^{-3}. However, we can take advantage of two facts: first, that individual single pulses from PSR J2251−3711 are considerably narrower than the integrated pulse (see Section 3.5), and second, that each of them acts as an *independent* DM estimator. Therefore, a large number of detectable single pulses can in principle be combined into a highly accurate DM estimator, within the 11 h worth of data in which the source is visible.

We therefore ran the HEIMDALL[1] single pulse search pipeline on all Parkes observations of PSR J2251−3711 with a narrow DM search step of 0.04 pc cm^{-3}. This returned a list of detected pulse DMs, signal-to-noise ratios (SNRs) and widths; the best reported width is that of the boxcar matched filter yielding the optimum response, noting that trial boxcar widths are equal to $2^k \times \tau$, where k is an integer in the range [1, 12] and $\tau = 64\,\mu s$ the time resolution of the data. After filtering out statistically insignificant events (SNR < 10), the remaining pulses showed a clearly bimodal distribution in DM, with RFI events clustering around zero and pulses from the source around ∼12 pc cm^{-3}. To completely eliminate any overlap between these two clusters, we also removed from the sample any pulse with a reported width $W > 10$ ms, which should not exclude many events originating from PSR J2251−3711. Finally, we removed all zero-DM events and a total of 326 pulses were left in our sample.

One missing ingredient here is the set of uncertainties on the reported single pulse DMs, but they can be inferred from the data as described below. We assumed them to be Gaussian with standard deviations σ_i proportional to the pulse widths w_i, which we choose to express as

$$\sigma_i = f \times \frac{w_i}{k_{\mathrm{DM}} \left(\nu_{\min}^{-2} - \nu_{\max}^{-2} \right)} \quad (1)$$

where $k_{\mathrm{DM}} = 4.148808 \times 10^3\ \mathrm{pc}^{-1}\,\mathrm{cm}^3\,\mathrm{MHz}^2\,\mathrm{s}$ is the dispersion constant, $\nu_{\min} = 1182$ MHz and $\nu_{\max} = 1523.4$ MHz are the bottom and top effective[2] observing frequencies expressed in MHz, w_i the reported pulse width in seconds, and f is a dimensionless, a priori unknown uncertainty scale factor to be fitted along other model parameters. In clearer terms, we have written that σ_i is proportional to the DM that corresponds to a dispersion delay w_i across the observing band.

Given the set of $n = 326$ observations (x_i, w_i, t_i), denoting respectively the observed DM, width, and MJD of detection of every pulse, the associated log-likelihood function can be written

$$\ln \mathcal{L}(d, \dot{d}, f) = -\sum_{i=1}^{n} \frac{\left(x_i - d - \dot{d}(t_i - t_{\mathrm{ref}}) \right)^2}{2\sigma_i^2} - \frac{1}{2} \sum_{i=1}^{n} \ln \left(2\pi\sigma_i^2 \right), \quad (2)$$

where d is the source DM, $\dot{d}$ the secular DM variation rate in pc cm^{-3} d^{-1}, and $t_{\mathrm{ref}} = 57\,900$ the reference MJD of the fit. The first term is essentially a reduced chi-square, and the second term places a penalty on higher values of f. We used the Markov chain Monte Carlo ensemble sampling package EMCEE (Foreman-Mackey et al. 2013) to estimate the joint posterior probability distribution of d, $\dot{d}$, and f (Fig. 2). We assumed uniform prior distributions for $\dot{d}$ and f, and a normally distributed prior for d mean and standard deviation given by the best DM and DM uncertainty reported by running pdmp on the folded main observation. We obtained $d = 12.12 \pm 0.01$ pc cm^{-3} with $f = 0.25 \pm 0.01$, and found no measurable secular DM variation (Fig. 2). We verified a posteriori the model assumptions by inspecting the fit residuals $\left(x_i - d - \dot{d}(t_i - t_{\mathrm{ref}}) \right) / \sigma_i$, which were found to have a median value of 0.03 and standard deviation of 1.0, i.e. consistent with the expected normal distribution.

[1] https://sourceforge.net/projects/heimdall-astro/
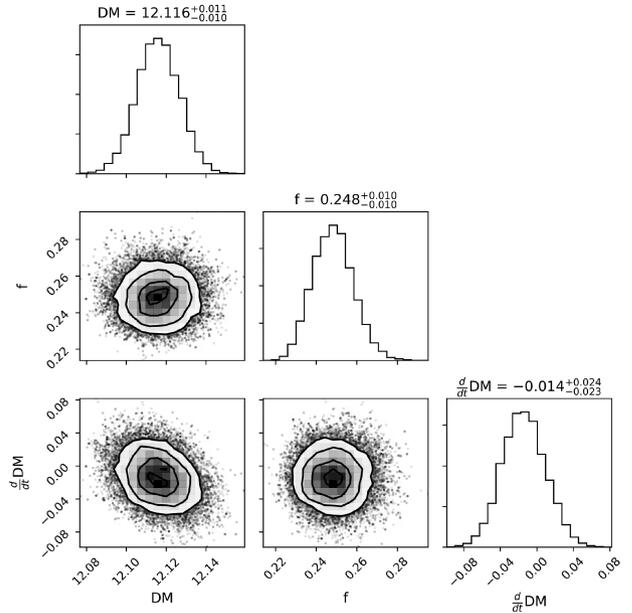[2] the top 58.6 MHz of the band are almost permanently occupied by RFI and were masked in the search.

Figure 2. Posterior probability densities for the source DM, DM rate of change (here in pc cm^{-3} yr^{-1}), and the dimensionless DM uncertainty scale factor f (see equation 1 and text for details). They were fitted to a sample of 326 single pulses detected by the search pipeline HEIMDALL across all Parkes multibeam observations of PSR J2251−3711. The lower and upper uncertainties quoted for all parameters correspond respectively to the 16th and 84th percentiles of their probability distributions.

From the DM value obtained, the Galactic electron density models NE2001 and YMW16 predict distances of 0.54 and 1.3 kpc, respectively. Considering that the distance to the pulsar is a key parameter when attempting to constrain its X-ray luminosity (see Section 4), this relative discrepancy is both large and unfortunate. On a sample of 189 known pulsars where a more reliable independent distance estimate is available, both NE2001 and YMW16 distance predictions were found to be inconsistent by a factor of 2 or more about 20 per cent of the time (fig. 14 of Yao et al. 2017). More recently, it has been shown from a sample of 57 pulsar parallaxes determined via very long baseline interferometry, that DM distances must be treated with even more caution for sources that are either nearby or at high Galactic latitudes (Deller et al. 2019). As PSR J2251−3711 arguably belongs to both categories, we need to remain open to the possibility that its distance may lie outside of the [0.5, 1.3] kpc range.

3.2 Timing analysis

All available observations were dedispersed at the DM determined in the analysis above and folded using dspsr (van Straten & Bailes 2011). We fitted a single von Mises[3] component to the integrated pulse profile of the main observation using the paas utility of PSRCHIVE, and the resulting noise-free pulse template was used to extract pulse TOAs from every folded observation. A total of 40 reliable TOAs were obtained, to which we fitted a phase-connected timing solution using TEMPO2 (Hobbs, Edwards & Manchester 2006). We limited the fit parameters to position, spin frequency, and spin frequency derivative, with the dispersion measure parameter

[3] a function defined on the unit circle, with a shape similar to a Gaussian.

Table 1. PSR J2251−3711 timing model and derived parameters. The dispersion measure was fitted on a large sample of single pulses (see Section 3.1 for details). The numbers in parentheses express the 1σ uncertainties on the last significant digit of each parameter.

Timing parameters	
Right ascension, α (J2000)	22:51:44.0(1)
Declination, δ (J2000)	−37:11:48(2)
Spin period, P (s)	12.122564931(1)
Spin period derivative, $\dot{P}$ (s s^{-1})	$1.310(4) \times 10^{-14}$
Dispersion measure, DM (pc cm^{-3})	12.12(1)
Spin frequency, ν (Hz)	0.082490793464(6)
Spin frequency derivative, $\dot{\nu}$ (Hz s^{-1})	$-8.91(3) \times 10^{-17}$
Epoch of timing solution (MJD)	57900
Timing span (MJD)	57363 − 58598
Number of TOAs	40
RMS timing residual (ms)	6.1
Solar system ephemeris model	DE430
Clock correction procedure	TT(TAI)
Derived parameters	
Galactic longitude, l (deg)	3.603
Galactic latitude, b (deg)	−62.882
NE2001 DM Distance (kpc)	0.54
YMW16 DM Distance (kpc)	1.3
Characteristic age (Myr)	14.7
Characteristic surface magnetic field (G)	1.3×10^{13}
Spin-down luminosity (erg s^{-1})	2.9×10^{29}

Figure 3. $P - \dot{P}$ diagram, based on v1.59 of the ATNF pulsar catalogue (Manchester et al. 2005). The period and period derivative ranges on the plot have been set to concentrate on the non-recycled pulsar population. The radio pulsars with the three longest spin periods have been highlighted in red. Lines of constant characteristic age and surface magnetic field strength are displayed in grey. The dashed red line represents the lower limit of the so-called pulsar death valley (equation 8 of Chen & Ruderman 1993). Death lines from Zhang et al. (2000) are also shown, based on their curvature radiation from vacuum gap model (green dashes) and space-charged-limited flow model (blue dashes).

being excluded and fixed to the value of DM = 12.12 pc cm^{-3} previously obtained. The resulting timing solution is presented in Table 1.

We note that the HTRU high-latitude survey detection of 2009 is significant enough to yield a TOA. It however deviates by approximately $\Delta t = 300$ ms from the time of arrival predicted by the ephemeris given in Table 1. Since Δt can in principle be further off an integer multiple of P, there is a non-negligible $2|\Delta t|/P \approx 5$ per cent probability for the TOA to fall within $|\Delta t|$ of the prediction by chance alone. We have therefore excluded it from this analysis. Including it in the fit yields P and $\dot{P}$ values consistent with those reported in Table 1 with uncertainties 5 times smaller, but this does not improve the positional uncertainty and more importantly does not enable an accurate fit for extra parameters such as proper motion or a second period derivative.

The location of PSR J2251−3711 on the $P - \dot{P}$ diagram is presented in Fig. 3, highlighted as a red cross. PSR J2251−3711 lies very near a region in which radio emission is predicted to shut down according to classical emission models (Chen & Ruderman 1993; Zhang, Harding & Muslimov 2000); however, it does not challenge these models to the same extent as radio pulsars PSR J0250+5854 (Tan et al. 2018) and PSR J2144−3933 (Young, Manchester & Johnston 1999), which have spin periods of 23.5 (longest known) and 8.5 s (third-longest known), respectively.

3.3 Long-term nulling

Within a single observation, the emission of PSR J2251−3711 is clearly sporadic, with more than half of its rotations showing no detectable pulse (Section 3.5). We therefore examined the entire SUPERB observation history to make an accurate census of non-detections of PSR J2251−3711, in order to determine if these could be attributed to its emission actually shutting down for an extended
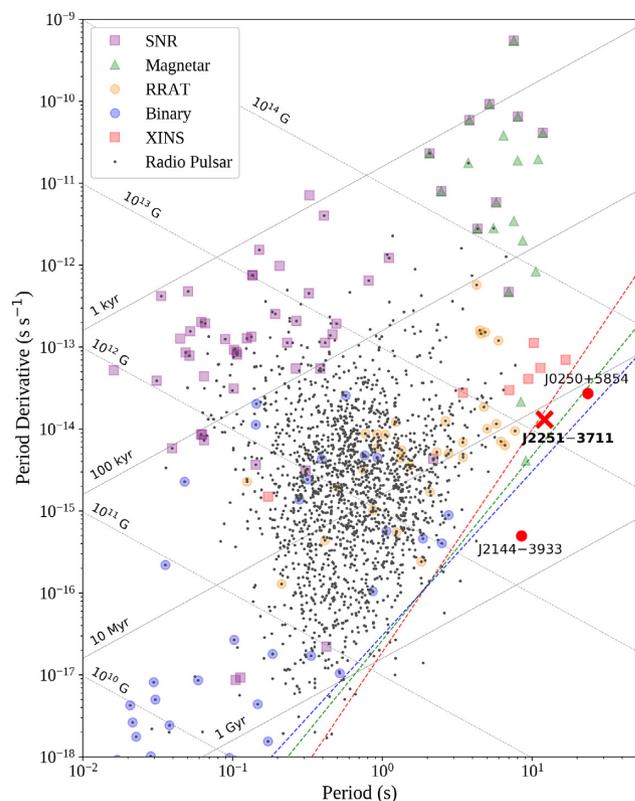
period of time. Among a total of 57 radio observations taken since its discovery, the source was bright enough to yield a valid TOA in 40 of them. We phase-coherently folded the remaining 17 using the ephemeris in Table 1 and examined the resulting output for the presence of pulses. We confirmed the presence of statistically significant pulses from the source in all but two observations, which were respectively 35 and 17 min long. We note however that in both cases the RFI environment was particularly adverse, enough that it was impossible to reliably determine the actual source of a pulse occurring within the phase window expected to be occupied by the pulsar. As a result, we cannot entirely rule out that PSR J2251−3711 would have been detected on both days had the observing conditions been quieter. Furthermore, and most importantly, the pulsar was successfully observed on the day following each of these non-detections. With the available data, we therefore find no compelling reason to believe that the radio emission from PSR J2251−3711 could cease for several hours or longer.

3.4 Mean polarization profiles

We used the 2-h long main observation to obtain the mean polarization profiles of the pulsar at 1382 MHz. Since the position angle
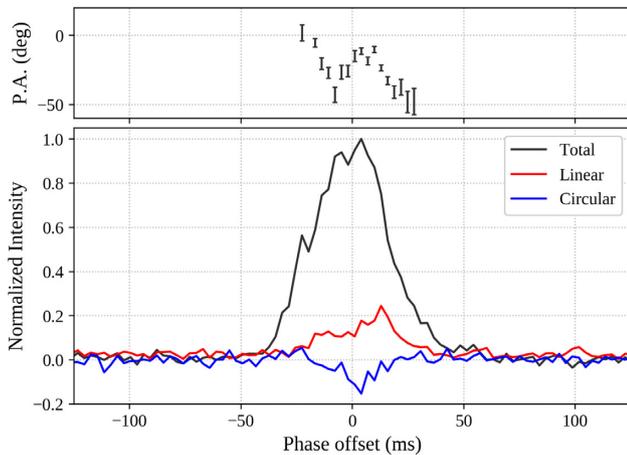
Figure 4. Bottom panel: mean polarization profiles at 1382 MHz, normalized to peak total intensity and corrected for Faraday rotation. Top panel: PA of the linearly polarized flux. Phase offset is measured from the peak of the Gaussian fit to the mean pulse intensity.

(PA) of the linearly polarized flux is affected by Faraday rotation when propagating through the interstellar medium, it is necessary to first evaluate the rotation measure (RM) of the pulsar in order to determine the intrinsic PA at the pulsar. We ran the `rmfit` utility of PSRCHIVE on every single pulse, thus obtaining a set of measured pulse RMs x_i, RM uncertainties σ_i, and SNRs. We filtered out statistically insignificant pulses and obvious outliers from the data set, and then inspected the remaining pulses to ensure that they were originating from the pulsar and not from an interference source. In the end, we were left with $n = 131$ reliable (x_i, σ_i) measurements. To determine the best-fitting RM of the source, we used a similar method to that used in determining the DM (Section 3.1). Our two fit parameters were the true rotation measure of the pulsar r and a dimensionless uncertainty scale factor f, introduced to take into account any potential systematic under or overestimation of the σ_i by the `rmfit` program. Ignoring constant terms, the log-likelihood of the data set is

$$\ln \mathcal{L}(r, f) = -n \ln f - \sum_{i=1}^{n} \frac{(x_i - r)^2}{2 f^2 \sigma_i^2}, \tag{3}$$

where we have postulated that the uncertainties on each pulse RM are normally distributed. Assuming uniform priors for r and f we obtained a best-fitting RM value of $r = 11 \pm 1$ rad m^{-2} and found that `rmfit` underestimated the uncertainties on every pulse RM by a factor $f = 1.6 \pm 0.1$. The fit residuals $(x_i - r)/(f\sigma_i)$ were consistent with the assumed normal distribution.

The mean polarization profiles of PSR J2251−3711 corrected for Faraday rotation are presented in Fig. 4, along with the PA of the polarized flux. The fractions of linear and circular polarization are 17 per cent and 6 per cent, respectively, within the pulse phase region, defined as phase bins with total intensity at least 3 times larger than the standard deviation of the background noise. However, the mean profiles do not capture the more complex characteristics observed in single pulses, which show a much higher degree of polarization and interesting, if not puzzling behaviour of the PA (Section 3.6). Using the SCIPY.OPTIMIZE PYTHON package, we found that the mean pulse intensity is well modelled by a single Gaussian component with a full width at half-maximum (FWHM) $W_{50} = 40.0 \pm 0.3$ ms. The corresponding full width

at ten per cent of the maximum is $W_{10} = 72.9 \pm 0.5$ ms. The average flux density of the pulsar at 1.4 GHz, estimated from the radiometer equation on this specific observation, is $S_{\mathrm{mean}} = 0.15$ mJy.

3.5 Single pulse intensity analysis

All single pulse intensities from the main observation are displayed in Fig. 5. At first glance, there is no clear evidence of sub-pulse drifting, as confirmed in a two-dimensional Fourier Transform of the single pulse stack. However, there was an indication of a systematic shift of pulse phase towards earlier time during this observation. A total drift of about 20 ms can clearly be seen directly in Fig. 5. To verify this statement we measured the phase of every single pulse, taken to be the phase of the boxcar matched filter that gives the best response when convolved with the pulse. Fitting a straight line to the single pulse phases (in units of time) as a function of time confirms that the drift rate r is statistically significant, with a value of $r = -3.6 \pm 0.6$ μs s^{-1}. This find was an incentive to carefully double check whether the data had been folded at an incorrect period due to the pulsar ephemeris being wrong, but no issues were found, and no timing residual exceeds 20 ms. This phase drift can therefore not persist indefinitely, or has to be periodic with a peak-to-peak amplitude no larger than approximately one integrated pulse width $W_{50} = 40$ ms, otherwise it would manifest itself as a detectable periodic signal in the timing residuals. The best-fitting total amount of drift in the main observation is $\Delta t = 26$ ms; if it was caused by an unmodelled movement of the source, it would correspond to a total line-of-sight (l.o.s.) displacement of $x = c\Delta t \simeq 8 \times 10^3$ km, which immediately rules out free precession of the pulsar as an explanation. The possibility of a binary companion then remains to be examined; if we assume that the pulsar follows a circular orbit, then the maximum l.o.s. orbital radius R that could credibly remain undetectable in the timing data is $R = cW_{50}/2$. Over the main observation, the pulsar would therefore have moved by approximately $x/2R \simeq 65$ per cent of an orbital diameter along the line of sight, implying that at least a quarter of the orbit has been covered, and therefore that the orbital period is no longer than 8 h. Further assuming that the orbit is edge-on, solving Kepler's third law yields a minimum companion mass $m = 5 \times 10^{-3}$ M$_\odot$, about five jovian masses. However, the accepted formation scenario for such tight binary systems involves the pulsar spun up to millisecond periods via accretion from a low-mass companion star, which appears quite unlikely here. The most reasonable explanation for the observed phase drift is therefore drifting sub-pulses over time-scales longer than 2 h. r might also be an alias of a higher drift rate associated with one or more drifting sub-pulse tracks, but the intermittency of the emission makes this impossible to determine.

We also obtained a pulse energy distribution by measuring the pulse signal-to-noise ratios on an identical phase window for all pulses. The width of the window was chosen to be twice the FWHM of the Gaussian fit to the integrated pulse intensity W_{50}, to ensure that all the signal originating from the pulsar was accounted for. Using the `pdistFit` utility of the PSRSALSA suite (Weltevrede 2016), we found that the pulse energy distribution is best fit by an exponential distribution with scale parameter $\lambda = 0.072$ modulated by a nulling probability of 65 per cent. The quantity $1/\lambda = 13.9$ represents the average S/N of pulses that are not nulls. Fig. 6 shows a comparison of both observed and fitted pulse energy cumulative distribution functions, which match closely.
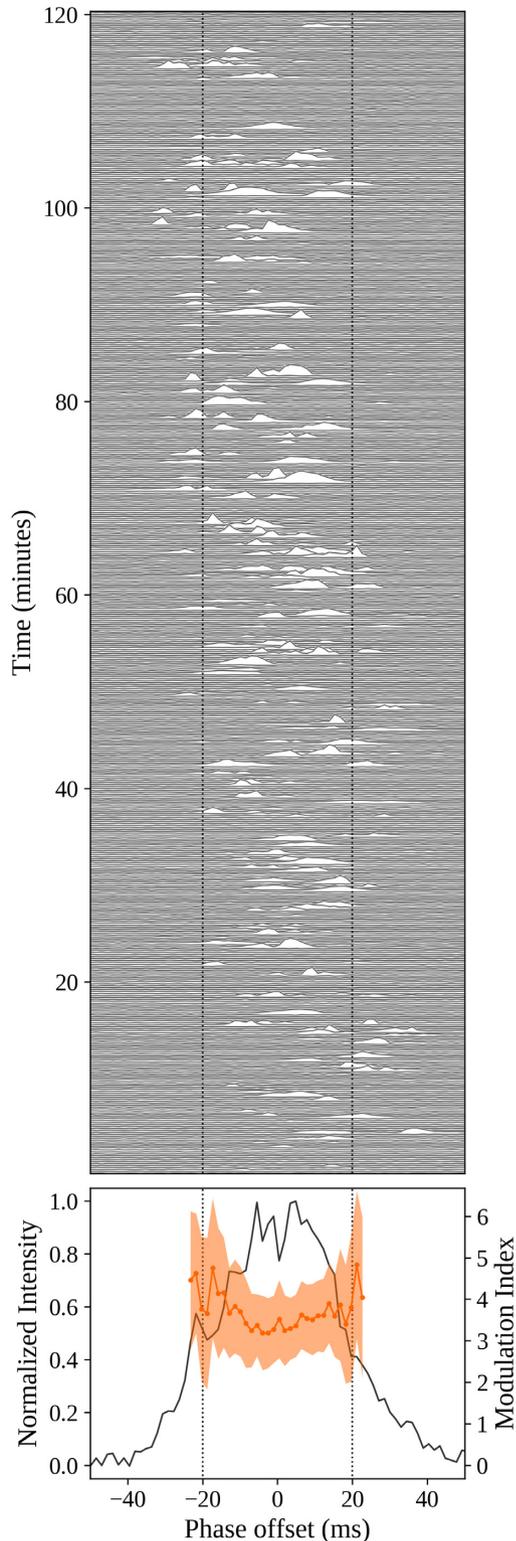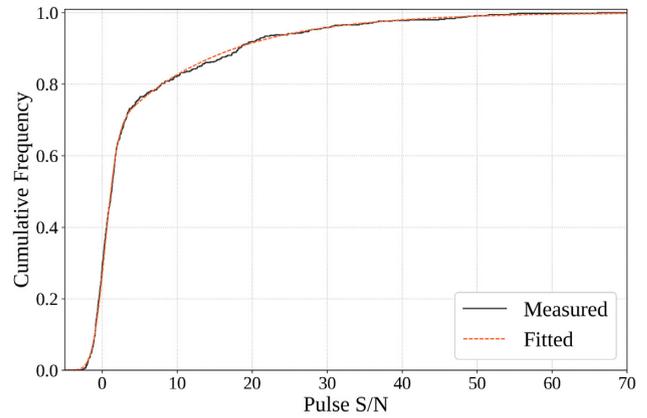
Figure 6. Cumulative distribution function of single pulse energies measured on the 2-h main observation (solid black line). S/N values are the integrated intensities of every pulse over an identical phase window, divided by the appropriate normalization factor. The intrinsic pulse energy distribution is well fitted by an exponential distribution modulated by a nulling probability of 65 per cent (dashed orange line).

3.6 Single pulse polarization

We examined the polarization profiles of all 596 single pulses, along with their phase-resolved PA curves. Many PA curves are difficult to individually exploit, due to being incomplete as a result of low signal-to-noise ratio, insufficient linear polarization, or simply the absence of emission in some phase ranges. Still, at least nine pulses show an uninterrupted 180-deg sweep of the PA with an S-shape similar to the rotating vector model (RVM; Radhakrishnan & Cooke 1969) prediction. The unusual fact here is that the sweep occurs at significantly different phases from one pulse to the other. We have shown four examples of single pulses to illustrate this behaviour in Fig. 7. Although some pulse periods show two or more well-spaced sub-pulses components, we note that there are no instances where two distinct 180-deg sweeps are observed. An RVM fit of the PA curve for these remarkable pulses does not provide any strong constraint on the emission beam geometry, due to a degeneracy between the angle between the spin and magnetic axes α, and the impact parameter of the line of sight β. But we note that in all single pulses where a fully sampled 180-deg rotation of the PA is visible, we consistently observe two characteristics. First, that the PA at the start of the sweep is close to zero degree. Secondly, that the PA monotonically decreases with phase; if one were to trust the RVM here, this would indicate that $\alpha > 90°$ and $\beta > 0°$, a so-called inner line of sight.

However, fully reconciling these observations with the RVM appears difficult. The main assumption of the RVM is that the direction of polarization is either parallel or orthogonal to the direction of the magnetic field at the point of emission; the field is taken to be strongly dipolar. A displacement of the point of emission along the plane orthogonal to the line of sight can explain a perceived delay (or advance) of the intensity curve, but should leave the PA curve invariant. It is then tempting to invoke changes of emission height between pulses, but the PA curve is expected to arrive $\Delta t = 4r/c$ later than the intensity curve, where r is the emission altitude (Blaskiewicz, Cordes & Wasserman 1991); clearly, both curves remain synchronized in all our pulses of interest, ruling out this explanation and requiring us to examine possible deviations from the RVM. In the radio pulsar population, the one most commonly observed is the so-called orthogonal polarization mode phenomenon
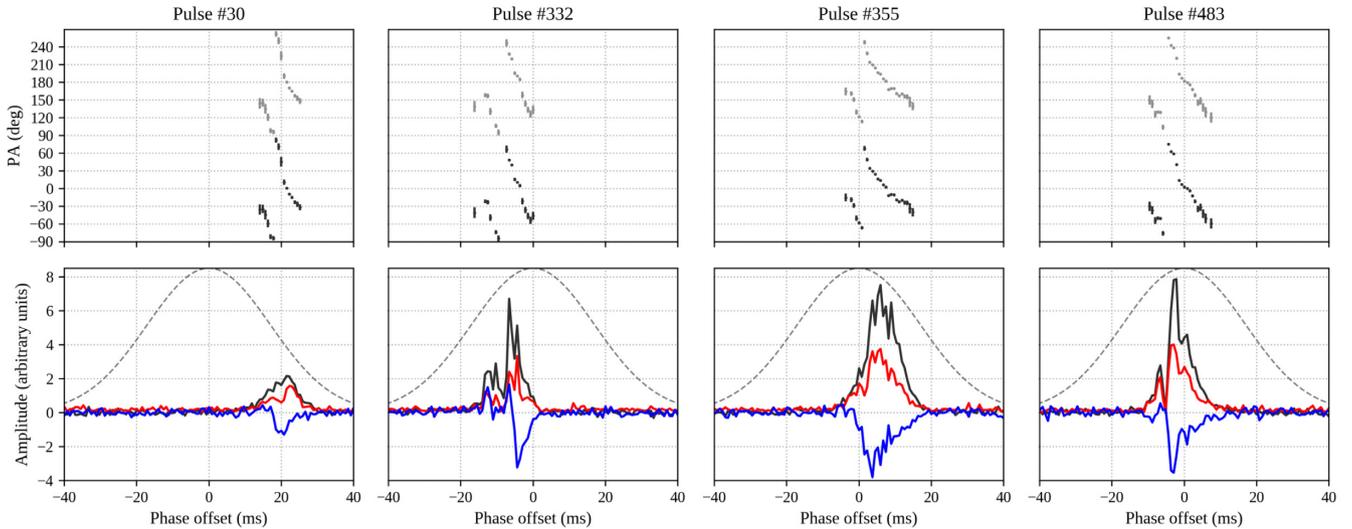

Figure 5. Top panel: single pulses from a continuous 2-h observation at a centre frequency of 1382 MHz. The vertical lines denote the FWHM of the Gaussian pulse fit. Bottom panel: Phase-resolved flux density (grey line, left axis) and modulation index (orange points, right axis) around the on-pulse region. The 1σ errors are represented by the shaded area. The overall tendency of single pulses to arrive earlier as the observation progresses is statistically significant (see text), and could be evidence for the presence of drifting sub-pulses tracks, wrapping around in phase on a time-scale of several hours.

Figure 7. Polarization profiles (at 1.4 GHz) of four example single pulses showing a smooth and uninterrupted 180-deg sweep of the PA *at different phases*. The time resolution of the data is 740 μs. Top panel: phase-resolved PA (black points) where the data are repeated a second time with a shift of 180 deg (grey points) for readability. Bottom panel: polarization profiles, with total intensity in black, linearly and circularly polarized flux in red and blue, respectively. The grey dashed line represents the best-fitting Gaussian to the integrated pulse intensity over the whole observation. Such continuous 180-deg rotation of the PA is somewhat reminiscent of the rotating vector model prediction for an inner line of sight (see text). However, the fact that the sweep occurs at different phases in every pulse is remarkable and difficult to explain. This behaviour is visible in a dozen pulses in the 2-h observation.

(OPM; e.g. Manchester, Taylor & Huguenin 1975), where the PA of one radiation mode follows the main RVM swing while the other is offset by 90 deg. Which mode is dominant can change as a function of pulse phase, causing so-called OPM transitions which register as 90-deg discontinuities in the PA. While OPMs do seem to be present in PSR J2251−3711, transitions between modes can hardly account for a full 180 deg worth of seemingly continuous PA rotation. If we were indeed to subtract 90 deg worth of OPM transition from the steepest part of each PA curve in Fig. 7, we would still be left with another 90 deg of residual smooth PA decrease that begins with an initial value of about 150 deg and occurs at different phases, which still cannot be interpreted in light of the RVM. To fully account for the rotation solely with OPMs, we would have to be observing unusually smooth forward then backwards OPM transitions in immediate succession, where the second transition is perceived as a 90-deg rotation of PA in the same direction as the first (rather than opposite direction as one may expect).

The time-shifted full-PA swings that are observed in the single pulses from PSR J2251−3711 may also be explainable by considering a multipolar nature for the pulsar's magnetic field structure. One expects, far from the stellar surface, the dipolar contribution to dominate, whereas near the surface quadrupole or higher order moments contribute. It is usually considered to be the case that the field is dipolar in all locations of interest relevant to pulsar emission, but in this case, with a remarkably slow pulsar, the potentially very large magnetosphere (the light cylinder radius is ∼600 000 km; for a 1-ms pulsar it would be ∼50 km) means that the higher multipoles may play an appreciable role. Any deviations from pure dipolar behaviour very close to the stellar surface mean that multiple tangential emission beams, each pointed differently, could exist. For such a large magnetosphere, the last closed field line encloses a small open field line region on the stellar surface such that if such a pulsar were observed at all then observing these multiple beams also might be more likely. Each individual beam would map out the same PA swing, but with relative time lags. We would expect to obtain

the same β and α values from RVM fits to each of the individual pulses, however as described above no constraining fit results when this is attempted. In this scenario, we would also expect to see some instances of two (or more) full PA swings per pulse period; our sample does not contain examples of this.

With simple ideas failing to conclusively account for what is observed, more advanced explanations may have to be envisaged. For example, that during the time taken by the line of sight to cross the emission region of a given single pulse, the observer perceives significant temporal evolution of the physical properties of the emission region; or, that polarization of the radiation is *not* determined at the point of emission, and is instead significantly altered by propagation effects through the magnetosphere (e.g. Beskin & Philippov 2012). But invoking unusual physical processes may not be the most appealing option, as one might argue that the 12-s rotation period of PSR J2251−3711 is not exceptional enough to justify why such processes would have not been observed before in other pulsars.

4 SEARCH FOR AN X-RAY COUNTERPART

4.1 Archival data

PSR J2251−3711 has similar spin-down parameters to those of XINSs (see Fig. 3), which show soft thermal X-ray emission and have spin periods $P \sim 3$–17 s. We therefore searched archival catalogues for an X-ray counterpart. The only potential match that we found is 2RXS J225144.6−371317 in the second *ROSAT* all-sky survey source catalogue (Boller et al. 2016), at a sky position of $\alpha = 22{:}51{:}44.69$, $\delta = -37{:}13{:}17.8$. The reported detection likelihood is 10.05, corresponding to a non-negligible probability of spurious detection of 14 per cent (table 1 of Boller et al. 2016), and the reported source count rate is $(5.8 \pm 2.0) \times 10^{-2}$ s^{-1}. This candidate source lies 1′.5 away from the radio pulsar. The typical 1σ position uncertainty of sources in the *ROSAT* catalogue is of the order of

0″.3, which suggests that 2RXS J225144.6−371317 is unlikely to be related to PSR J2251−3711.

For an absorbed blackbody model, the best-fitting temperature reported in the catalogue for this candidate source is $kT = 22 \pm 3000$ eV; the disproportionately large uncertainty suggests that the fitting procedure failed and that the output value should not be trusted. The best-fitting hydrogen column density $N_\mathrm{H} = (2.2 \pm 160) \times 10^{20}$ cm^{-2} suffers the same problem, but at least appears consistent with what is expected from the DM−N_H relationship of He, Ng & Kaspi ([2013]) and a hypothetical source DM = 7 pc cm^{-3} (entirely reasonable for this line of sight). We can trust however that the spectral shape of the *ROSAT* source is quite soft, since all 19 source counts were detected in the lowest energy band 100–440 eV. This is consistent with thermal emission from an XINS, of which all known specimens have blackbody temperatures kT between 50 and 107 eV (table 3 of Viganò et al. [2013]). Converting[4] the *ROSAT* count rate into an unabsorbed bolometric luminosity yields $L_\mathrm{2RXS}^{85\,\mathrm{eV}} = 1.2 \times 10^{32}\,(d/1\,\mathrm{kpc})^2$ erg s^{-1}, where d is the distance to the source and where we have assumed $kT = 85$ eV, the average XINS temperature. This is compatible with known XINS luminosities (Viganò et al. [2013]), providing additional incentive to re-observe the field.

4.2 *Swift* observations

In an attempt to detect the pulsar in the soft X-ray band, we obtained a total of $T_\mathrm{obs} = 4.4$ ks of exposure time with the *Neil Gehrels Swift Observatory* X-Ray Telescope (*Swift* XRT), which covers the 0.3–10 keV band. The observations were taken on 2019 May 5th and 8th (Target ID: 00011329), with the field centred on the position of the *ROSAT* source discussed above. We stacked the observations and analysed the resulting image, shown in Fig. 8. Around the pulsar's timing position (Table 1), no counts were detected within the 9 arcsec half-power radius of the *Swift* XRT point spread function (PSF). From this we can infer, using table 3 of Kraft, Burrows & Nousek ([1991]), an upper bound at the 99 per cent confidence level on the total source counts (within the PSF) $\lambda_{S,u} = 4.6$, and an associated count rate $R_{S,u} = \lambda_{S,u}/T_\mathrm{obs} = 1.03 \times 10^{-3}$ s^{-1}. In order to convert to an unabsorbed bolometric thermal luminosity, we need an estimate of the hydrogen column density, which we set to $N_\mathrm{H} = 3.7 \times 10^{20}$ cm^{-2} based on the DM−N_H relationship of He et al. ([2013]). Assuming a blackbody source model with the average temperature of known XINS $kT = 85$ eV, $R_{S,u}$ corresponds to an unabsorbed bolometric thermal luminosity of $L_{S,u}^{85\mathrm{eV}} = 1.1 \times 10^{31}\,(d/1\,\mathrm{kpc})^2$ erg s^{-1}, where d is the distance to the pulsar. This luminosity (at $d = 1$ kpc) corresponds to the lower end of the XINS luminosity distribution. We note, however, that the upper bound thus derived is sensitive to the postulated source temperature; using the lowest reported XINS temperature ($kT = 50$ eV) instead yields a value 5 times larger $L_{S,u}^{50\mathrm{eV}} = 5.3 \times 10^{31}\,(d/1\,\mathrm{kpc})^2$ erg s^{-1}, close to the median XINS luminosity.

In this *Swift* exposure, it is interesting to note that a source is detected with a significance level of 4.5σ (4 counts) within 35 arcsec of the position of 2RXS J225144.6−371317. Given the *ROSAT* positional uncertainty of 20 arcsec and the *Swift* XRT PSF half-power radius of 9 arcsec, attributing both detections to the same underlying source is tempting. However, we first need to

---

[4]For such conversion purposes, we used the *WebPIMMS* mission count rate simulator throughout this section: https://heasarc.gsfc.nasa.gov/cgi-bin/Tools/w3pimms/w3pimms.pl.

examine our second set of X-ray observations before attempting a fully informed interpretation of the field (see Section 4.4).

4.3 NICER observations

We also performed follow-up observations of PSR J2251−3711 with the *Neutron star Interior Composition Explorer* (*NICER*), an X-ray observatory attached in 2017 to the International Space Station. The *NICER* X-ray timing instrument is non-imaging, has a field of view of 6 arcmin and covers the soft X-ray energy range 0.2–12 keV with a large effective area (1900 cm^2 at 1.5 keV) and high time resolution ($\lesssim 100$ ns). It is therefore well suited to the observation of potential XINS. Observations were taken from 2017 December 18 through 2018 June 14, spanning observation IDs 1020650101–102065014 and a net exposure time of 62 ks. For spectroscopic investigations using the non-imaging detectors, the *NICER* team have developed two different background modelling methods: the space-weather (SW) model and 3C 50 model. We used optimized filtering criteria for each model to select good time intervals of low particle and optical loading backgrounds and exclude noisy detector modules. After this filtering process, the X-ray spectra showed weak residuals below 1 keV using either background model. The filtered and background-subtracted 0.3–1 keV count rates were 0.019(3) and 0.056(4) counts s^{-1}, corresponding to 7 per cent and 23 per cent of the background count rate for the SW and 3C 50 background models, respectively.

Fitting the time-averaged, background-subtracted *NICER* spectra with an absorbed blackbody model, we found temperatures $kT = 86 \pm 11$ eV and 96 ± 7 eV, emission radii $R = 0.84$km$(d/1$ kpc), and $R = 1.0$km$(d/1$ kpc) for the SW and 3C 50 background models, respectively. These correspond to absorbed X-ray fluxes in the 0.3–1 keV band of $2.0^{+0.1}_{-1.3} \times 10^{-14}$ and $5.6^{+0.8}_{-0.7} \times 10^{-14}$ erg s^{-1} cm^{-2}, respectively. Converting them to unabsorbed luminosities at $d = 1$ kpc assuming the hydrogen column density previously postulated for the pulsar yields $7.7^{+0.4}_{-5.0} \times 10^{30}$ and $1.8^{+0.3}_{-0.2} \times 10^{31}$ erg s^{-1} cm^{-2}, respectively. The first value is compatible with the 99 per cent confidence upper bound previously placed on PSR J2251−3711's luminosity for a similar temperature of $kT = 85$ eV, but the second is about 60 per cent larger, suggesting that the majority of the *NICER* counts do *not* originate from the pulsar.

None the less, we searched barycentric corrected X-ray events for pulsations at the spin period measured for PSR J2251−3711 from radio timing data. We did not find any significant signal in the 0.3–1.0 keV band. After subtraction of background contributions assuming the SW and 3C 50 models, 3σ upper limits on the intrinsic source pulsed fraction were estimated to be 100 per cent and 88 per cent for these two models, respectively. In the former case, the low source count rate makes any pulsation undetectable even if the emission was 100 per cent pulsed.

4.4 Interpreting the field

Overall there are three tentative X-ray band detections in the field: an integrated *NICER* spectrum, a *ROSAT* catalogue source, and a 4-count cluster in a 4.4-ks *Swift* exposure. All three are of limited statistical significance, which precludes any categorical interpretations of the data. Also, due to the relatively large 3 arcmin radius of the *NICER* field of view, the provenance of the photons it collected needs to be considered. We can at least rule out the possibility of 2RXS J225144.6−371317 being a steady thermal source with a temperature in the range of known XINS. Indeed, the luminosity inferred from the *ROSAT* source count rate lies far above
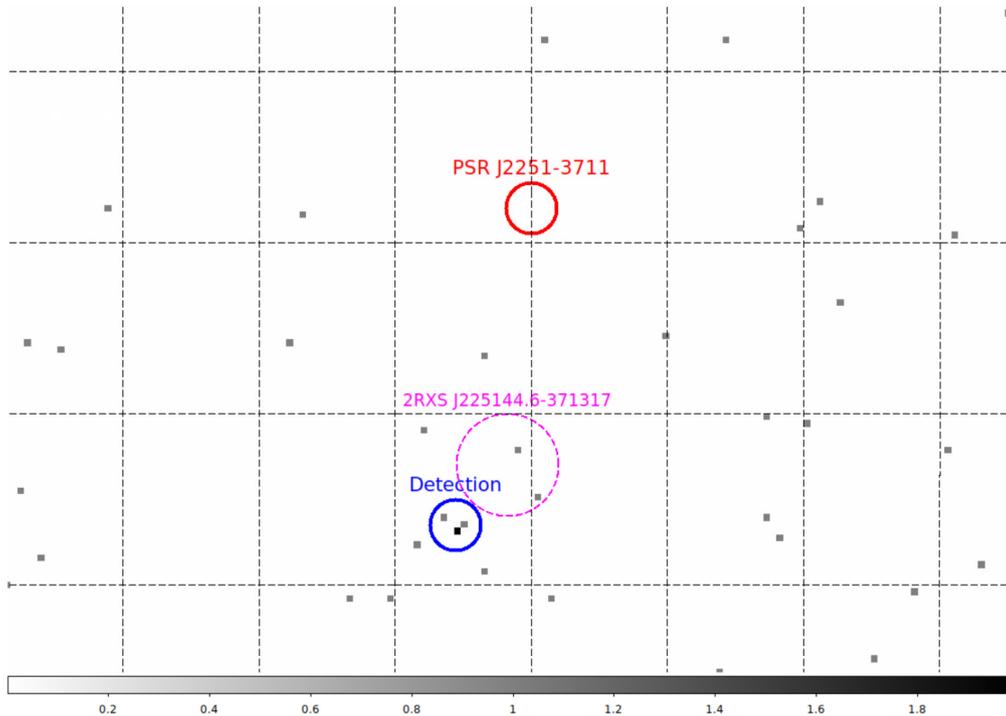
Figure 8. *Swift* X-ray image of the field, with a total exposure time of 4.4 ks. Only a zoom on the region of interest is shown. The coordinate grid spacing is 1 arcmin on both RA (horizontal) and Dec. (vertical) axes. Red circle: half power diameter (18 arcsec) of the *Swift* PSF centred on the radio timing position of PSR J2251−3711, enclosing zero counts. Blue circle: a 4-count detection with a statistical significance of 4.5σ. Magenta dashed circle: the 1σ position uncertainty on the original detection of the *ROSAT* faint source 2RXS J225144.6−371317.

the detection thresholds of our observations; the source should have manifested itself in the *Swift* observation as dozens of counts and registered a detectable blackbody spectrum in any individual *NICER* exposure. It remains possible to reconcile the parameters reported by *ROSAT* with the absence of a clear *Swift* detection, if we assume that its temperature kT is lower than 35 eV. Otherwise, 2RXS J225144.6−371317 is either a variable source that remained in a quiet state during our observation campaign (2017 December to 2019 May), or the original *ROSAT* detection was spurious.

The 4-count detection in the *Swift* exposure could be a more interesting case, being coincident to 4 arcsec with a star of magnitude 21 in the *Gaia* data release 2 (Gaia Collaboration 2018, Source ID: 6547998120327478272). No further data (e.g. parallax or spectral type) are currently available for this object. If it is responsible for the X-ray counts, then it would likely be too bright in the optical to be an INS, and too faint in the X-ray band to be part of an X-ray binary.

In any case, no candidate source in the field appears to be bright enough to single-handedly account for the *NICER* blackbody-shaped spectrum. The most reasonable explanation is that the *NICER* spectrum originates from other background sources. The *Swift* observation currently provides the best constraint on PSR J2251−3711's X-ray luminosity.

5 DISCUSSION

5.1 Nature of PSR J2251−3711

Considering the position of PSR J2251−3711 in the $P − \dot{P}$ diagram, its possible relationship to X-ray emitting neutron star

classes deserves to be examined. We can certainly exclude that PSR J2251−3711 is an active magnetar, as the typical X-ray luminosity of such an object (10^{33}–10^{36} erg s^{-1}, Olausen & Kaspi 2014) would have been easily detected in our data; but the idea of PSR J2251−3711 being a low-B magnetar similar to SGR 0418+5729 (Rea et al. 2010) or Swift J1822.3−1606 (Livingstone et al. 2011) seems plausible at first sight. All three objects share very similar spin characteristics, which is evident from Fig. 3. SGR 0418+5729 could have credibly remained undetected in our observations (even placed at a 1 kpc distance) given its X-ray flux in quiescence of less than a few 10^{-14} erg cm^{-2} s^{-1} (Rea et al. 2013), which would be consistent with the non-detection of our pulsar. However, most magnetars are either radio quiet, or show particularly wide radio profiles with duty cycles in excess of 10 per cent with significant time variability, which may include weeks to months of nulling (Camilo et al. 2008; Levin et al. 2010). This makes a magnetar classification for PSR J2251−3711 much less credible. Furthermore, its high Galactic latitude ($b = −62.9°$) stands in stark contrast to the magnetar population, although we will expand on this specific point below.

On the other hand, there are no strong arguments against PSR J2251−3711 being an XINS. Its period, period derivative, Galactic latitude and distance all appear compatible with that of known thermally emitting INSs. The main question here is of course the non-detection of the pulsar in the X-ray band. The 99 per cent confidence upper bound on its bolometric unabsorbed thermal luminosity, derived in the previous section, is $L_{S,u}^{85eV} = 1.1 \times 10^{31}$ erg s^{-1} assuming that it lies at a distance of 1 kpc. This luminosity is comparable to that of RX J0420.0−5022 and RX J1605.3+3249, the two faintest known XINS. One must however take into account

a margin of error of nearly an order of magnitude on this upper bound, due to uncertainties on the distance to the PSR J2251−3711 and its unknown temperature. Furthermore, we can consider its X-ray over spin-down luminosity ratio $L_X/\dot{E}$, which provides another useful means of distinguishing between neutron star classes; see e.g. fig. 12 of Enoto, Kisaka & Shibata (2019) for an up-to-date $L_X − \dot{E}$ diagram of the neutron star population. For all reasonable distance and temperature estimates, the upper bound on $L_X/\dot{E}$ for PSR J2251−3711 remains larger than 1, compared to a value of $\lesssim 0.01$ that would be required to confidently place it in into the rotation-powered pulsar category. It is therefore currently not possible to rule out an XINS nature for PSR J2251−3711. The matter will only be settled with observations using sensitive X-ray observatories with imaging capabilities, such as *XMM–Newton* or the *Chandra X-ray Observatory*.

5.2 Evolution history of PSR J2251−3711

There are two plausible and quite distinct evolution scenarios for PSR J2251−3711 that we shall discuss here. The first is that it followed the standard picture, where it would have been born with parameters similar to those of the Crab pulsar and have undergone a spin-down evolution dominated by magnetic dipole braking. In this case, its true age should be comparable to its characteristic age of 15 Myr. There are however significant caveats to the dipole braking model, especially when the task at hand is to determine the age of a radio pulsar. First, the model assumes that the inclination angle α between the spin and magnetic axes remains constant, while there is some observational evidence that both axes tend to align over time (Tauris & Manchester 1998). Such decrease of α manifests itself as an increased braking index n (Tauris & Konar 2001), potentially giving the illusion of a decreasing characteristic surface magnetic field if $n > 3$. Secondly, the accurately known braking indices (noted n hereafter) for young pulsars are in the range −1.2 to 3.2 (Archibald et al. 2016; Espinoza, Lyne & Stappers 2017); this suggests that pulsars are born with $n < 3$, which corresponds to an increase of the characteristic surface magnetic field (either apparent or possibly physical, Espinoza et al. 2011; Ho 2015). Taking into account these two extra ingredients, namely a plausible distribution of braking indices at birth and a negative $\dot{\alpha}$ term, Johnston & Karastergiou (2017) managed to reproduce the bulk of the $P–\dot{P}$ diagram population of isolated NS. Interestingly, their model postulated that the intrinsic magnetic field of pulsars does *not* decay. Among their conclusions was that the characteristic age is then a systematic overestimate of the true age. We can infer from their fig. 5 that a pulsar with a characteristic age of 15 Myr born in the same $P–\dot{P}$ region as the Crab should see its true age estimate reduced by half an order of magnitude, to approximately 4 Myr.

The alternative evolution scenario for PSR J2251−3711 is that it started its neutron star life as a magnetar. It is generally accepted that the high energy emission of a magnetar is powered by the dissipation of its magnetic field; in strongly magnetized neutron stars ($B \gtrsim 10^{13}$ G), it has been shown that the time evolution of the temperature and magnetic field of the star strongly depend on each other and must be treated simultaneously (Aguilera, Pons & Miralles 2008; Pons, Miralles & Geppert 2009). This has sparked the development of so-called magnetothermal evolution models of neutron stars, the most advanced being that of Viganò et al. (2013) which provides a number of directly testable predictions, in particular the trajectory that a neutron star follows in the $P–\dot{P}$ diagram as it cools down. The amount of magnetic field decay over

time depends strongly on the initial magnetic field configuration postulated for the star, which could be exclusively crustal (their model A), or with a significant core component (their models B and C). In the latter case, the dipole component of the magnetic field is shown to remain approximately constant, and there $n = 3$ braking is expected as above, also corresponding to an age of several Myr. But an initially crustal field decays significantly over time, which is accompanied by a rapid spin-down as shown in their fig. 10. It therefore appears plausible that PSR J2251−3711 was born as 'model A' magnetar with an initial dipolar surface magnetic field strength $B \simeq 3 \times 10^{14}$ G, which, if we are to trust the model of Viganò et al. (2013), would make it approximately 0.4 Myr old.

Choosing between evolution models with or without magnetic field decay for PSR J2251−3711 clearly rests upon obtaining an estimate of its true age, given that they predict ages that differ by an order of magnitude. The detection of an X-ray counterpart would be direct evidence that the pulsar is younger than the typical NS cooling time of 1 Myr and would strongly argue in favour of a magnetar origin. The unusually high Galactic latitude of PSR J2251−3711 might also provide another means of estimating its true age; if we assume that its parent supernova occurred in the Galactic plane, then a lower bound on the vertical component of its kick velocity would be

$$v_z = 870 \left(\frac{d}{\text{kpc}} \right) \left(\frac{T}{\text{Myr}} \right)^{-1} \text{ km s}^{-1}, \tag{4}$$

where d is the present distance to the pulsar and T its age. The velocity component transverse to our line of sight would have approximately half ($\cos b = 0.46$) the value above. The resulting observable proper motion further away from the Galactic plane would then be

$$|\dot{b}| = 84 \left(\frac{T}{\text{Myr}} \right)^{-1} \text{ mas yr}^{-1}. \tag{5}$$

The young age of ≈ 0.4 Myr predicted by model A of Viganò et al. (2013) may therefore manifest itself through a proper motion close to the highest values currently known for a radio pulsar (Manchester et al. 2005). Timing at 1.4 GHz is unlikely to ever yield a measurable proper motion due to the high timing residuals of the source, which currently limits positional accuracy to a few arcseconds; long baseline radio interferometry is therefore required. An alternative would be to estimate the velocity of PSR J2251−3711 relative to the interstellar medium from measurements of its diffractive scintillation time and frequency scales (e.g. Cordes & Rickett 1998; Johnston, Nicastro & Koribalski 1998); the source is not bright enough in our radio data to make such a measurement practical, but the prospects of doing so with a more sensitive facility such as MeerKAT are very good. We note as a caveat to this discussion that a nearby neutron star such as PSR J2251−3711 may have been born significantly out of the Galactic plane, due to the presence of a significant number of potential progenitors off the plane within a 1 kpc radius – the so-called OB runaway stars (Posselt et al. 2008).

In summary, it is possible to find evidence that PSR J2251−3711 is young, but no such direct avenues exist to demonstrate that it is old. Confirmation of old age would instead likely be found in a persistent lack of evidence for youth in future observations, in both radio and X-ray bands.

6 CONCLUSION

We have presented radio and X-ray observations of PSR J2251−3711, a newly discovered radio pulsar with an unusually long spin period of 12.1 s, the second largest known. Its radio emission is intermittent with a ∼65 per cent nulling fraction, but it does not appear to shut down on time-scales of hours or days. It shows a small sample of single pulses with 180-deg sweeps of the polarization PA, that remarkably occurs at different phases from one pulse to the other. This observation cannot be easily reconciled with the rotating vector model, but we have suggested a few tentative explanations to be further explored. We have also shown that PSR J2251−3711 is unlikely to be a low-B magnetar; however, the possibility of it being a cooling XINS remains open, which must be tested with deeper X-ray imaging observations.

PSR J2251−3711 lies in a region of the $P − \dot{P}$ diagram predicted to be a magnetar graveyard by magnetothermal evolution models, but that same region could also credibly contain ordinary (and much older) radio pulsars that underwent a spin-down evolution with little to no magnetic field decay. It will be interesting in the near future to determine which evolutionary paths the emerging population of very slow radio pulsars ($P > 10$ s) actually followed. This should hopefully bring new constraints to magnetothermal evolution models and overall contribute to a unified vision of the apparent neutron star diversity.

REFERENCES

Aguilera D. N., Pons J. A., Miralles J. A., 2008, ApJ, 673, L167
Archibald R. F. et al., 2016, ApJ, 819, L16
Beskin V. S., Philippov A. A., 2012, MNRAS, 425, 814
Bhattacharya D., van den Heuvel E. P. J., 1991, Phys. Rep., 203, 1
Blaskiewicz M., Cordes J. M., Wasserman I., 1991, ApJ, 370, 643
Boller T., Freyberg M. J., Trümper J., Haberl F., Voges W., Nandra K., 2016, A&A, 588, A103
Burrows D. N. et al., 2005, Space Sci. Rev., 120, 165
Camilo F., Reynolds J., Johnston S., Halpern J. P., Ransom S. M., 2008, ApJ, 679, 681
Camilo F., Ransom S. M., Chatterjee S., Johnston S., Demorest P., 2012, ApJ, 746, 63
Chen K., Ruderman M., 1993, ApJ, 402, 264
Cordes J. M., Lazio T. J. W., 2002, preprint (arXiv:astro-ph/0207156)
Cordes J. M., Rickett B. J., 1998, ApJ, 507, 846
Deller A. T. et al., 2019, ApJ, 875, 100
Enoto T., Kisaka S., Shibata S., 2019, Rep. Prog. Phys., 82, 106901
Espinoza C. M., Lyne A. G., Kramer M., Manchester R. N., Kaspi V. M., 2011, ApJ, 741, L13
Espinoza C. M., Lyne A. G., Stappers B. W., 2017, MNRAS, 466, 147
Foreman-Mackey D., Hogg D. W., Lang D., Goodman J., 2013, PASP, 125, 306
Gaensler B. M., Frail D. A., 2000, Nature, 406, 158
Gaia Collaboration, 2018, A&A, 616, A1
He C., Ng C.-Y., Kaspi V. M., 2013, ApJ, 768, 64
Hessels J. W. T., Ransom S. M., Stairs I. H., Freire P. C. C., Kaspi V. M., Camilo F., 2006, Science, 311, 1901
Ho W. C. G., 2015, MNRAS, 452, 845
Hobbs G. B., Edwards R. T., Manchester R. N., 2006, MNRAS, 369, 655
Hotan A. W., van Straten W., Manchester R. N., 2004, Publ. Astron. Soc. Aust., 21, 302
Johnston S., Karastergiou A., 2017, MNRAS, 467, 3493
Johnston S., Nicastro L., Koribalski B., 1998, MNRAS, 297, 108
Kaspi V. M., 2010, Proc. Natl. Acad. Sci., 107, 7147
Kaspi V. M., Beloborodov A. M., 2017, ARA&A, 55, 261
Kaspi V. M., Kramer M., 2016, preprint (arXiv:1602.07738)
Keane E. F. F., 2018, MNRAS, 473, 116
Keane E. F., Kramer M., 2008, MNRAS, 391, 2009
Keane E. F., Ludovici D. A., Eatough R. P., Kramer M., Lyne A. G., McLaughlin M. A., Stappers B. W., 2010, MNRAS, 401, 1057
Keane E. F., McLaughlin M. A., Kramer M., Stappers B. W., Bassa C. G., Purver M. B., Weltevrede P., 2013, ApJ, 764, 180
Keith M. J. et al., 2010, MNRAS, 409, 619
Kondratiev V. I., McLaughlin M. A., Lorimer D. R., Burgay M., Possenti A., Turolla R., Popov S. B., Zane S., 2009, ApJ, 702, 692
Kraft R. P., Burrows D. N., Nousek J. A., 1991, ApJ, 374, 344
Kramer M., Lyne A. G., Hobbs G., Löhmer O., Carr P., Jordan C., Wolszczan A., 2003, ApJ, 593, L31
Kramer M., Lyne A. G., O'Brien J. T., Jordan C. A., Lorimer D. R., 2006, Science, 312, 549
Levin L. et al., 2010, ApJ, 721, L33
Livingstone M. A., Scholz P., Kaspi V. M., Ng C. Y., Gavriil F. P., 2011, ApJ, 743, L38
Lyne A., Graham-Smith F., 2012, Pulsar Astronomy. Cambridge Univ. Press, Cambridge, UK
Lyne A. G., Jordan C. A., Graham-Smith F., Espinoza C. M., Stappers B. W., Weltevrede P., 2015, MNRAS, 446, 857
Manchester R. N., Taylor J. H., Huguenin G. R., 1975, ApJ, 196, 83
Manchester R. N., Hobbs G. B., Teoh A., Hobbs M., 2005, AJ, 129, 1993
Noutsos A., Schnitzeler D. H. F. M., Keane E. F., Kramer M., Johnston S., 2013, MNRAS, 430, 2281
Olausen S. A., Kaspi V. M., 2014, ApJS, 212, 6
Patterson J., 1979, ApJ, 234, 978
Pons J. A., Miralles J. A., Geppert U., 2009, A&A, 496, 207
Posselt B., Popov S. B., Haberl F., Trümper J., Turolla R., Neuhäuser R., 2008, A&A, 482, 617
Potekhin A. Y., Pons J. A., Page D., 2015, Space Sci. Rev., 191, 239
Radhakrishnan V., Cooke D. J., 1969, Astrophys. Lett., 3, 225
Rea N. et al., 2010, Science, 330, 944
Rea N. et al., 2013, ApJ, 770, 65
Rigoselli M., Mereghetti S., Suleimanov V., Potekhin A. Y., Turolla R., Taverna R., Pintore F., 2019, A&A, 627, A69
Staveley-Smith L. et al., 1996, Publ. Astron. Soc. Aust., 13, 243
Tan C. M. et al., 2018, ApJ, 866, 54
Tauris T. M., Konar S., 2001, A&A, 376, 543

Tauris T. M., Manchester R. N., 1998, MNRAS, 298, 625

Thompson C., Duncan R. C., 1995, MNRAS, 275, 255

Turolla R., 2009, in Becker W., ed., Neutron Stars and Pulsars, Isolated Neutron Stars: The Challenge of Simplicity. Springer Berlin Heidelberg, New York, p. 141

van Straten W., Bailes M., 2011, Publ. Astron. Soc. Aust., 28, 1

Viganò D., Rea N., Pons J. A., Perna R., Aguilera D. N., Miralles J. A., 2013, MNRAS, 434, 123

Weltevrede P., 2016, A&A, 590, A109

Yao J. M., Manchester R. N., Wang N., 2017, ApJ, 835, 29

Young M. D., Manchester R. N., Johnston S., 1999, Nature, 400, 848

Young N. J., Weltevrede P., Stappers B. W., Lyne A. G., Kramer M., 2014, MNRAS, 442, 2519

Zhang B., Harding A. K., Muslimov A. G., 2000, ApJ, 531, L135

This paper has been typeset from a TeX/LaTeX file prepared by the author.